The flow-induced sound of a wall-mounted finite length cylinder with circular and square cross-section

Danielle J. Moreau*and Con J. Doolan†

The University of Adelaide, South Australia, Australia 5005

This paper presents the results of an experimental investigation of the sound produced by flow interaction with a wall-mounted finite length cylinder of circular or square cross-section. Acoustic measurements have been taken in an anechoic wind tunnel at a range of flow speeds and for a wide variety of aspect ratios (cylinder length to diameter ratio). Unsteady velocity data have also been measured in the cylinder wake using hot-wire anemometry and these data are related to far-field noise measurements to determine the flow mechanisms responsible for noise generation. Cylinder aspect ratio was found to be an important parameter that controls vortex shedding behaviour and hence tonal noise generation. Multiple peaks in the noise spectra can be attributed to different vortex cells in the near wake, the number and strength of which are controlled by aspect ratio influencing flow over the tip or cylinder-wall junction.

I. Introduction

Aerodynamic sound is a major component of the noise produced by modern air, road and rail vehicles. The sound generated by cylindrical objects in cross-flow is an important source of this flow-induced noise as cylindrical objects are found in aircraft landing gear, rail pantographs and automobile appendages. In fact, cylindrical geometries can be found in a variety of applications such as cooling stacks, high-rise buildings, bridge piers, chimneys, masts and pipelines. As flow-induced cylinder noise is relevant to a wide range of applications, it is important that the governing noise generation mechanisms are well understood so that the noise radiated into the far-field can be minimised.

The majority of studies on flow-induced cylinder noise have focused on Aeolian tone generation from two-dimensional cylinders in uniform cross-flow.[1–10] In comparison, only one study has been conducted on the sound generated by flow over a wall-mounted finite length cylinder. This is despite the fact that most real world applications use finite length cylinders.

The flow field around a wall-mounted finite length cylinder features a variety of complex and three-dimensional fluid phenomena. In addition to the alternating spanwise vortex shedding (Karman vortex street) observed for a two-dimensional cylinder, end effects are also present. A pair of counter-rotating vortex structures form at the cylinder tip, associated with downwash over the cylinder free-end.[11–13] In the lower boundary layer, a U shaped horseshoe vortex system is present around the cylinder base and extends into the wake.[14] Additionally, a pair of counter-rotating base vortex structures form in the lower part of the wake, close to the cylinder-wall junction, due to upward-directed flow at the cylinder base.[15–18] These vortex systems may merge and interact, resulting in a complex wake structure.

For a wall-mounted finite length cylinder in low Mach number flows, the flow structure and hence the radiated sound will depend on Reynolds number, aspect ratio (L/D, where L is cylinder length and D is diameter) and the ratio between the cylinder length and the wall boundary layer thickness. Lee[12] reported that at high aspect ratio, Karman vortex shedding along the cylinder span has a cellular structure that reduces with aspect ratio. For circular cylinders with $L/D > 12$, three or more cells of Karman vortex shedding were observed and this reduced to two cells when $7 < L/D < 12$ and to a single cell along the entire cylinder span when $L/D < 7$. At very low cylinder aspect ratio, end effects have been shown to have an influence over the entire cylinder span. In this case, downwash and tip vortices may suppress periodic

*Postdoctoral Research Associate, School of Mechanical Engineering, danielle.moreau@adelaide.edu.au, AIAA member

†Associate Professor, School of Mechanical Engineering, con.doolan@adelaide.edu.au, AIAA Senior member

Karman vortex shedding from the cylinder sides and instead, arch vortices form on the ground plane in the cylinder near wake. The aspect ratio at which this occurs varies between studies but is generally found to be between $L/D = 1$ and 7.[12, 16, 19, 20]

King and Pfizenmaier[21] are one of only two to experimentally investigate the sound produced by finite length cylinders in cross-flow. Their study obtained noise measurements for cylinders of various cross-section (circular, elliptical and square) and aspect ratio (L/D = 2 - 35) in a free jet at Reynolds numbers of $Re_D = 4.2 \times 10^4 - 1.3 \times 10^5$, based on cylinder diameter. Aspect ratio was found to be an important parameter in determining the peak frequency and sound level of the radiated noise. In addition, cylinders with an elliptical cross-section were identified as producing the lowest overall noise levels. Becker et al.[22] are the only prior study who have examined the flow around and noise produced by a wall-mounted finite length square cylinder with aspect ratio of $L/D = 6$ at Reynolds numbers of $Re_D = 1.3 \times 10^4 - 3.8 \times 10^4$. They examined the effect of attaching different shaped fore- and afterbodies to the square cylinder on the flow field and radiated noise. Adding a wedge shaped body to the square cylinder leading edge was found to give the largest reductions in aerodynamic noise due to the creation of flow instabilities that break up spanwise vortex shedding from the cylinder sides.

Published information on the flow-induced-noise mechanisms of wall-mounted finite length cylinders is scarce. In particular, no prior study has examined noise measurements for a wide variety of cylinder aspect ratios nor has any study investigated different cylinder shapes or how aspect ratio and geometry affect spanwise vortex shedding and noise. This paper presents the results of an original experimental investigation of flow induced noise of wall-mounted finite length cylinders. It presents, for the first time, flow and noise data for circular and square cylinders with a variety of aspect ratios (L/D = 1.6 - 22.6 for the circular cylinder and L/D = 0.97 - 13.6 for the square cylinder) and at a range of Reynolds numbers ($Re_D = 1.0 \times 10^4 - 1.4 \times 10^4$ for the circular cylinder and $Re_D = 1.6 \times 10^4 - 2.4 \times 10^4$ for the square cylinder). In addition, this study identifies the flow mechanisms responsible for the most prominent spectral information in the noise data. This paper is structured as follows: Section II presents the experimental method; Section III presents the far-field acoustic and wake velocity data; and the paper is concluded in Section IV.

II. Experimental setup

A. Anechoic wind tunnel facility

Experiments were performed in the anechoic wind tunnel at the University of Adelaide. The anechoic wind tunnel test chamber is 1.4 m × 1.4 m × 1.6 m (internal dimensions) and has walls that are acoustically treated with foam wedges to approximate a free-field environment at frequencies above 250 Hz. The facility contains a contraction outlet that is rectangular in cross-section with dimensions of 75 mm x 275 mm. The maximum flow velocity of the free jet is $\sim$ 40 m/s and the free-stream turbulence intensity is 0.33%.[23]

B. Test models

The cylinders were fixed (one at a time) to a side plate which was in turn flush mounted to the contraction flange so that the cylinder length axis was perpendicular to the direction of the flow, as shown in Fig. 1. The aluminum side plate has a length of 300 mm in the streamwise direction and a width of 155 mm in the vertical direction. As shown in Fig. 1, the centre of the cylinder is positioned 30 mm downstream of the jet exit plane at the vertical centreline of the jet.

A total of 28 circular cylinders were used in this study: 14 cylinders have a circular cross-section with a diameter of $D = 6$ mm and 14 cylinders have a square cross-section with dimensions of 10 mm ×10 mm. The 14 square and circular cylinders each have a length, L, between δ and 14δ, where δ is the boundary layer thickness on the side plate at the cylinder location at $U_\infty = 35$ m/s. The side plate boundary layer thickness, δ, at the cylinder location was measured prior to the cylinder being attached to the side plate and was found to be 9.7 mm (see Section II D). The circular cylinders have an aspect ratio of between $L/D = 1.6$ and 22.6 and the thickness of the boundary layer to cylinder diameter is $\delta/D = 1.6$. The square cylinders have an aspect ratio between $L/D = 0.97$ and 13.6 (where in this case, D refers to the width of the square cylinder cross-section) and $\delta/D = 0.97$.

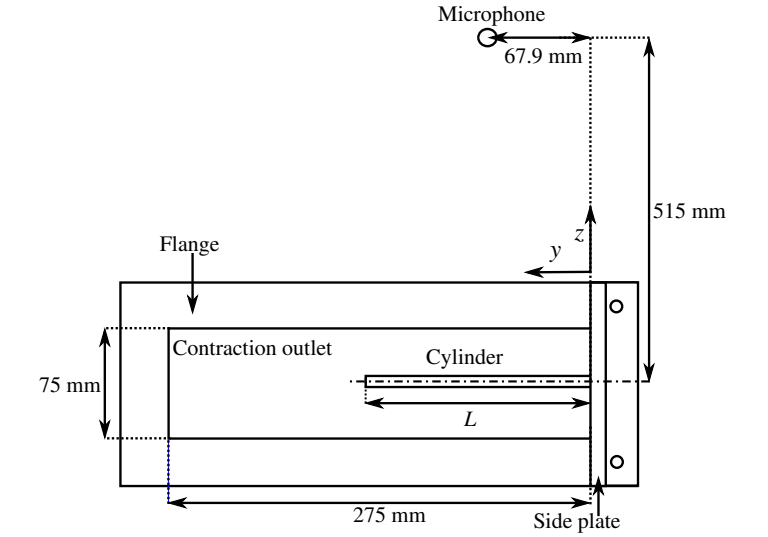

(a) Side view.

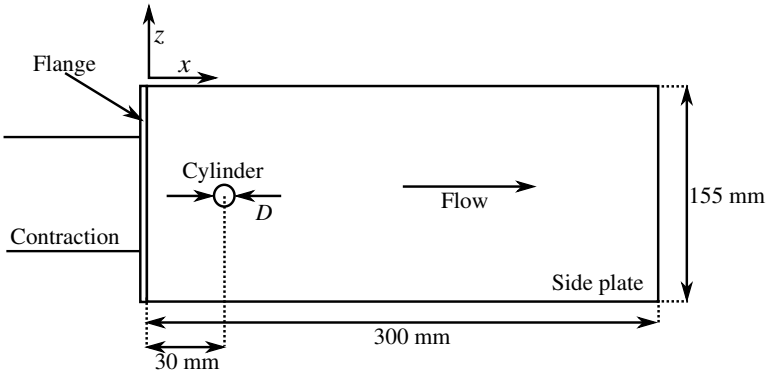

(b) Front view

Figure 1: Schematic diagram of the circular cylinder in the anechoic wind tunnel test section.

C. Measurement equipment and procedure

Acoustic measurements were recorded with each of the cylinders mounted (one at a time) to the side plate. Noise data were measured at a single observer location using a B&K 1/2" microphone (Model No. 4190) located 515 mm directly above the centre span of the longest cylinder with $L = 14\delta$. To provide isolation from wind noise caused by very low level recirculation in the anechoic chamber, a wind sock was placed on the microphone prior to data collection. The accuracy in the microphone sound pressure level measurements is ± 1 dB (as stated by the manufacturer).

Hot-wire anemometry was used to obtain unsteady velocity data in the wake of the cylinders. A TSI 1210-T1.5 single wire probe with wire length of $L = 1.27$ mm and a wire diameter of $d = 3.81$ μm was used. The sensor was connected to a TSI IFA300 constant temperature anemometer system and positioned using a Dantec automatic traverse with 6.25 μm positional accuracy. The traverse allowed continuous movement in the streamwise (x), spanwise (y) and vertical (z) directions. The co-ordinate system used in this study is shown in Fig. 1.

Experiments were conducted at three flow speeds between $U_\infty = 25$ and 35 m/s corresponding to Reynolds numbers of $Re_D = 1.0 \times 10^4 - 1.4 \times 10^4$ for the circular cylinder and $Re_D = 1.6 \times 10^4 - 2.4 \times 10^4$ for the square cylinder. The flow around a cylinder is generally classified into three regimes: subcritical ($Re_D = 2 \times 10^2 - 1 \times 10^5$), supercritical ($Re_D = 1 \times 10^5 - 4 \times 10^6$) and transcritical ($Re_D > 4 \times 10^6$).[24] Therefore in this study, measurements are taken for finite length cylinders with circular and square cross-section at

subcritical Reynolds numbers.

Acoustic and flow data were recorded for each flat plate model using a National Instruments board at a sampling frequency of 5×10^4 Hz for a sample time of 8 s. All data are presented in narrow band format with a frequency resolution of 1 Hz.

D. Side plate boundary layer characteristics

The side plate boundary layer mean velocity profile ($\overline{U}/U_\infty$) at the cylinder location at $U_\infty = 35$ m/s is shown in Fig. 2 (a). In this figure, the mean velocity profile is compared with the 1/7th power law for a turbulent boundary layer and the Blasius boundary layer solution for laminar flow. Figure 2 (a) shows that the side plate boundary layer approximates the 1/7th power law profile indicating that the flow is well developed and in a turbulent state on the side plate at the cylinder location. At this measurement location, the boundary layer thickness, calculated as the distance from the side plate to the point where the flow velocity has reached 99% of the free-stream velocity, is $\delta = 9.7$ mm.

The turbulent nature of a boundary layer can be confirmed via analysis. A turbulent boundary layer profile may be expressed in terms of non-dimensional velocity, u^+, and distance, y^+, defined as

$$u^+ = \frac{U}{u_\tau} = f_1(y^+), \tag{1}$$

$$y^+ = \frac{y u_\tau}{\nu}, \tag{2}$$

where the friction velocity $u_\tau = \sqrt{\tau_w/\rho}$, τ_w is the wall shear stress, ρ is the fluid density and ν is the kinematic viscosity. In the very near-wall region, the viscosity dominates and

$$u^+ = y^+. \tag{3}$$

Further from the wall, the law of the wall (or log-law) comes into effect and

$$u^+ = 1/\kappa \ln(y^+) + B, \tag{4}$$

where typically, constants $\kappa = 0.41$ and $B = 5$.

For a turbulent boundary layer on a smooth flat plate, the skin friction coefficient, c_f, can be approximated as[25]

$$c_f = \frac{0.059}{Re_x^{1/5}}, \tag{5}$$

and is related to the wall shear stress, τ_w, according to

$$c_f = \frac{\tau_w}{\frac{1}{2}\rho U_\infty^2}. \tag{6}$$

Figure 2 (b) shows the non-dimensionalised side plate mean velocity profile at $U_\infty = 35$ m/s collapses along the law of the wall indicating a turbulent boundary layer.

The side plate boundary layer normalised rms velocity profile ($\overline{u}'/U_\infty$) at the cylinder location at $U_\infty = 35$ m/s is shown in Fig. 2 (c). This figure shows that the turbulent energy is at a maximum in the inner boundary layer region at $y = 1.5$ mm above the plate surface. After this point, there is a reduction in the turbulent energy in the outer boundary layer and in the free-stream.

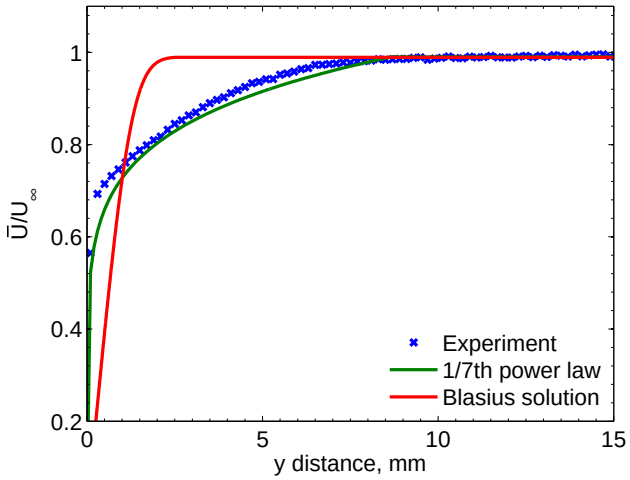

(a) Normalised mean velocity profile.

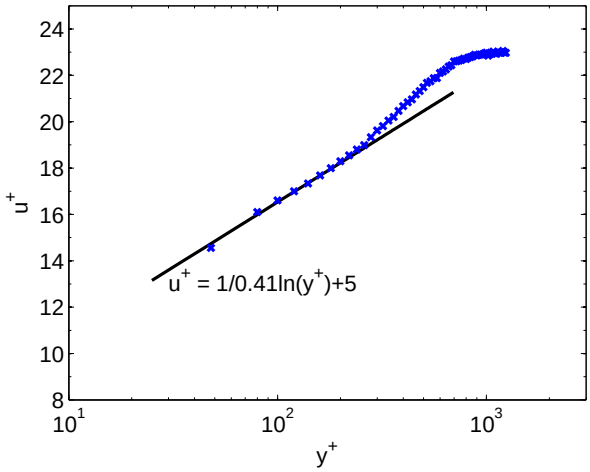

(b)

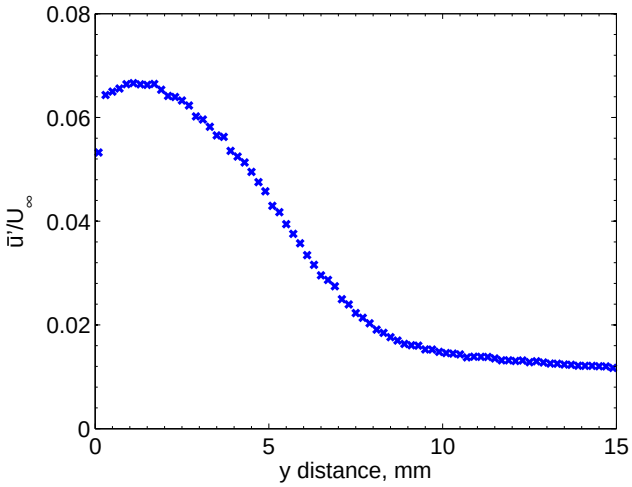

(c) Normalised rms velocity profile.

Figure 2: Side plate boundary layer profiles at the cylinder location for $U_\infty = 35$ m/s. (a) Normalised mean velocity profile compared to the 1/7th power law profile and the Blasius solution, (b) non-dimensionalised mean velocity profile compared to the law of the wall and (c) normalised rms velocity profile.

III. Experimental results

A. Acoustic measurements

1. *Far-field acoustic spectra*

Figures 3 and 4 show 2D spectral maps of the noise produced by the circular and square cylinders at $U_\infty = 25$ and 35 m/s. For closer inspection, Figs. 5 and 6 show single line acoustic spectra for cylinders with selected aspect ratios at $U_\infty = 25$ - 35 m/s.

Figures 3 - 6 show that aspect ratio is an important parameter that affects the spectral content of noise radiated by the cylinders in cross-flow. This parameter determines how or whether vortices are shed from the cylinder sides resulting in acoustic tone generation. For all cylinder geometries, reducing the flow speed from $U_\infty = 35$ to 25 m/s has the effect of reducing the peak frequency of any tonal noise components and the magnitude of the radiated sound.

At the highest aspect ratio of $L/D = 22.6$, Figs. 3 and 5 (a) show that a high amplitude double vortex

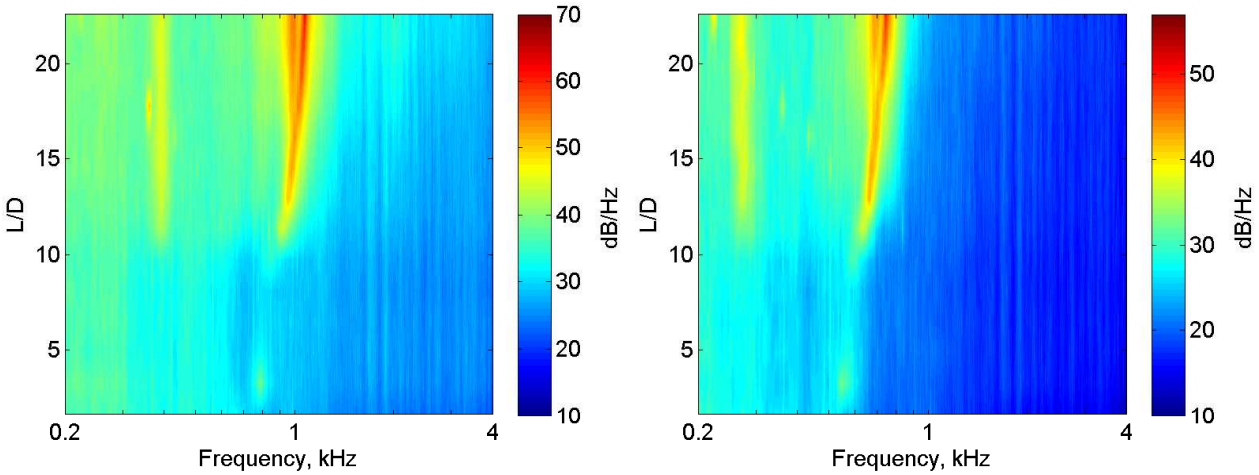

(a) $U_\infty = 35$ m/s.

(b) $U_\infty = 25$ m/s.

Figure 3: Far-field acoustic spectral maps for the circular cylinders. Note the differing colorbar scales.

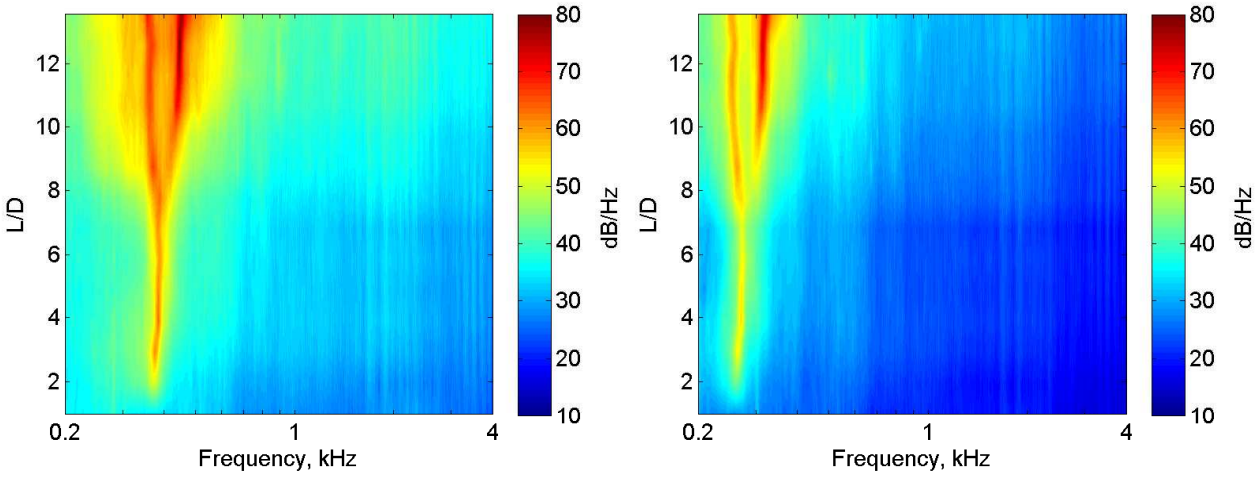

(a) $U_\infty = 35$ m/s.

(b) $U_\infty = 25$ m/s.

Figure 4: Far-field acoustic spectral maps for the square cylinders. Note the differing colorbar scales.

shedding peak is observed in the circular cylinder noise spectra. This double peak (referred to as a dominant double peak hereafter) remains visible in the noise measurements for circular cylinders with an aspect ratio down to and including $L/D = 19.4$. A broad dominant double peak is also observed in noise spectra for the square cylinder when its aspect ratio is between $L/D = 13.6$ and 8.7 (see Figs. 4 and 6 (a)).

When the aspect ratio of the circular cylinder is reduced to $L/D = 17.8$ (the next highest aspect ratio after $L/D = 19.4$), the dominant double peak observed at a higher aspect ratio becomes a single peak in the noise spectra. This single vortex shedding peak (referred to as the dominant single peak hereafter) is observed for circular cylinders with an aspect ratio between $L/D = 9.7$ and 17.8 (see Figs. 3 and 5 (b)). A dominant single peak is similarly observed in the square cylinder noise spectra when its aspect ratio is between $L/D = 7.8$ and 1.9 (see Figs. 4 and 6 (b)).

The dominant double and single peaks produced by the circular cylinder with aspect ratio between $L/D = 9.7$ and 22.6 are accompanied by a low amplitude, low frequency secondary peak (e.g. at 394 Hz when $U_\infty = 35$ m/s in Figs. 3 (a) and 5 (a) and (b)). No secondary peak is observed in the square cylinder noise spectra.

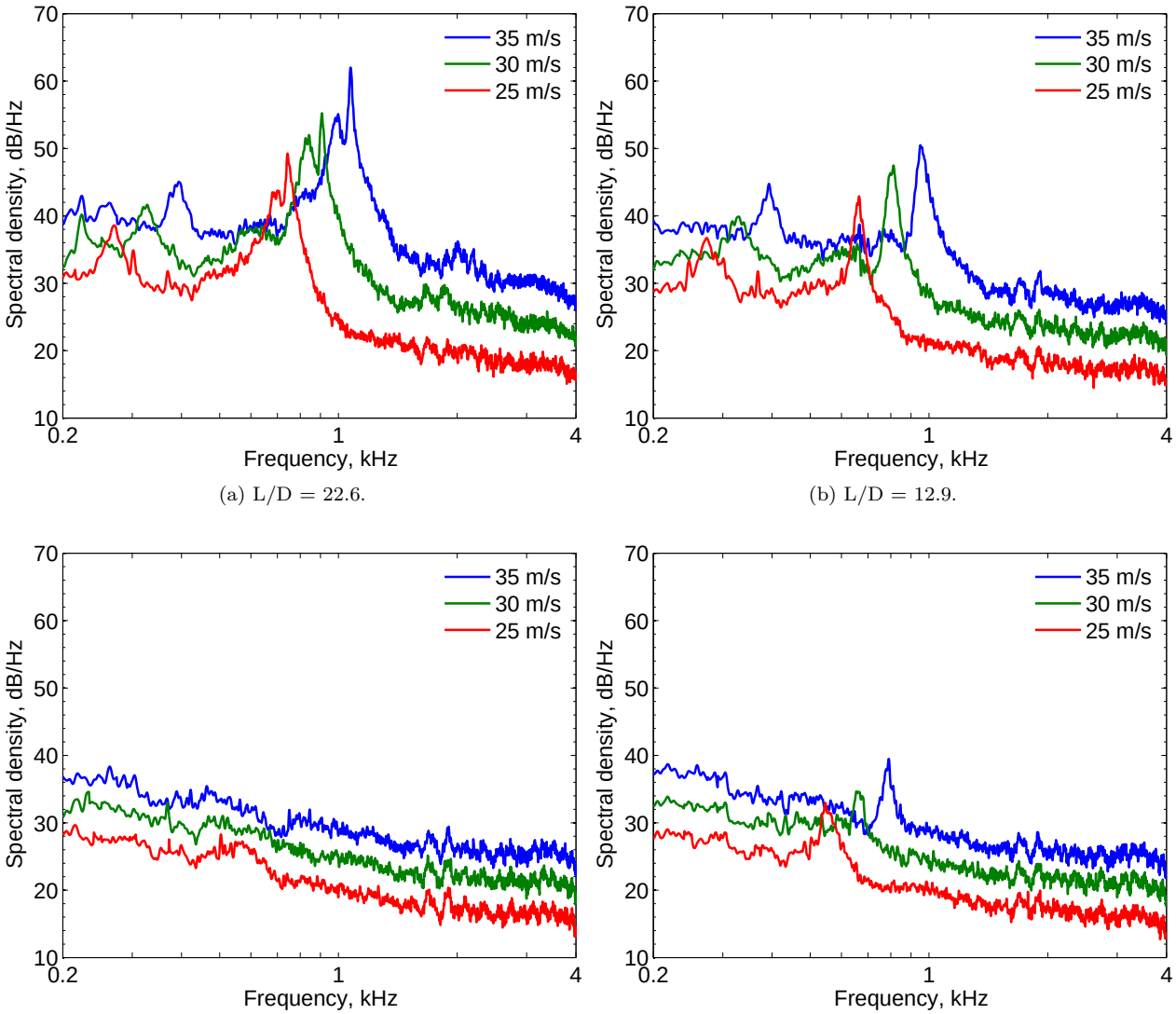

(a) L/D = 22.6.

(b) L/D = 12.9.

(c) L/D = 6.5.

(d) L/D = 3.2.

Figure 5: Far-field acoustic spectra for the circular cylinders at U_∞ = 25 - 35 m/s.

No peaks are observed in the noise spectra for circular cylinders with an aspect ratio between $L/D = 4.9$ and 8.1 (see Figs. 3 and 5 (c)) and for the square cylinder when $L/D = 0.97$ (see Figs. 4 and 6 (c)). In this case, vortex shedding has been suppressed from the sides of the cylinder, preventing acoustic tone generation. Interestingly, a single peak reappears in the noise spectra for the circular cylinder when its aspect ratio is $L/D = 3.2$ (see Figs. 3 and 5 (d)). The magnitude of the peak is low indicating that the vortex shedding process responsible is weak. When the circular cylinder aspect ratio is further reduced to $L/D = 1.6$, no peaks are observed in the noise spectra and the sound produced is entirely broadband in nature (see Fig. 3).

Figure 7 provides a summary of the dominant peaks observed in the circular and square cylinder noise spectra at flow speeds of U_∞ = 25 - 35 m/s. This figure shows that acoustic tones are produced by the square cylinder with a much lower aspect ratio than the cylinder with circular cross section. The noise radiation remains low and broadband in nature when the aspect ratio of the circular cylinder is between $L/D = 4.9$ and 8.1 or is below 1.6. While for the square cylinder, the aspect ratio must be below $L/D = 1$ to prevent acoustic tone generation.

Previous studies on the flow structure around wall-mounted finite height cylinders have found a critical aspect ratio to exist below which Karman type vortex structures are suppressed and replaced with arch

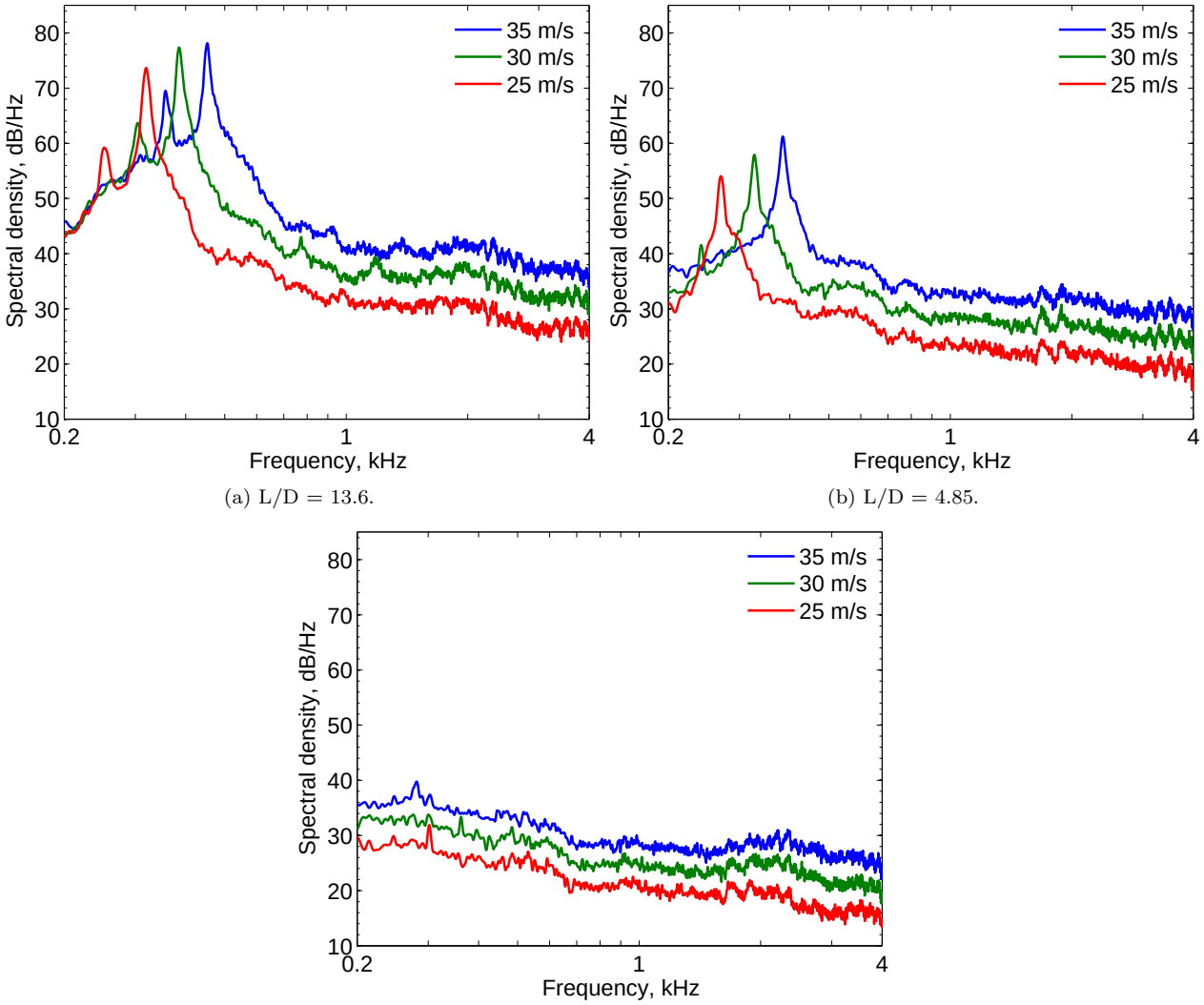

(a) L/D = 13.6.

(b) L/D = 4.85.

(c) L/D = 0.97.

Figure 6: Far-field acoustic spectra for the square cylinders at U_∞ = 25 - 35 m/s.

vortices on the ground plane in the near wake. The critical aspect ratio varies between studies but is generally found to be between $L/D = 1$ and 7[11,16,19] which is in agreement with the experimental results of Fig. 7. Discrepancies in the critical aspect ratio are attributed to differences in the relative thickness of the boundary layer to cylinder geometry, δ/D and δ/L.[16]

2. *Overall sound pressure level*

Figure 8 shows the variation in overall sound pressure level with aspect ratio for the circular and square cylinders at flow speeds between $U_\infty = 25$ and 35 m/s. This figure shows that for both cylinder geometries, increasing the the flow speed from $U_\infty = 25$ to 35 m/s has the effect of increasing the overall noise levels. The overall sound pressure levels are shown to increase with cylinder aspect ratio except between $L/D = 3.2$ and 8.1 for the circular cylinder and between $L/D = 2.9$ and 6.8 for the square cylinder, when the noise levels remain fairly constant. The highest noise levels are recorded for cylinders with the highest aspect ratio, when a dominant double peak is observed in their noise spectra. Conversely, the lowest overall sound levels are produced by cylinders with the lowest aspect ratio, when no acoustic tone is produced.

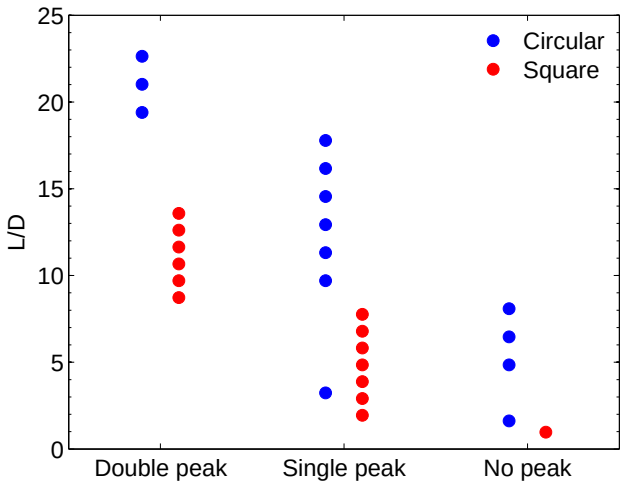

Figure 7: Dominant peaks observed in the noise spectra for the circular and square cylinders at $U_\infty = 25$ - 35 m/s.

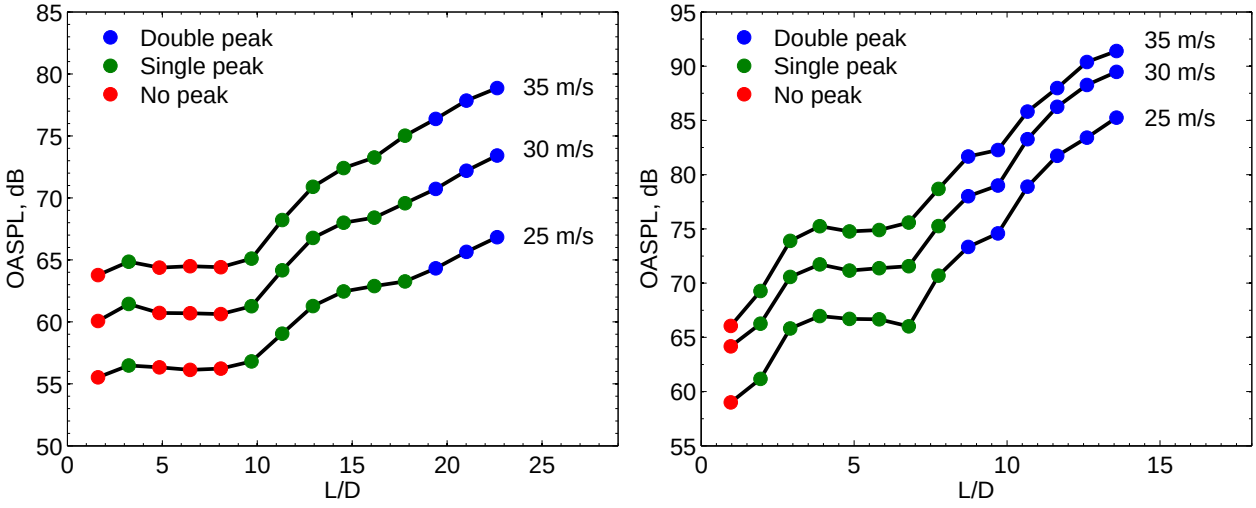

(a) Circular cylinder.

(b) Square cylinder.

Figure 8: Overall sound pressure level variation for the circular and square cylinder at $U_\infty = 25 - 35$ m/s. Note the differing scales.

3. Acoustic scaling

Curle[1] showed that the noise radiation characteristic of a cylinder is dipole like. The dipole sound is related to the unsteady forces created by fluid flow on the cylinder surface. Therefore, cylinder noise is expected to scale with M^6 where M is the free-stream Mach number. The spectra for the circular and square cylinders with selected aspect ratios at $U_\infty = 25 - 35$ m/s are normalised by M^6 in Fig. 9 according to:

$$\text{Scaled spectral density} = \text{spectral density} - 60\log_{10}(M). \tag{7}$$

In Fig. 9, the scaled cylinder noise spectra are plotted against the nondimensional Strouhal number, St_D, based on cylinder diameter, D. Figure 9 shows that an M^6 power law gives a good collapse of the noise spectra for both the circular and square cylinder at flow speeds between $U_\infty = 25$ and 35 m/s. Spectral data that are originally spread by almost 45 dB are collapsed to within 8 dB. Both cylinder geometries

therefore behave as acoustical dipoles and radiate sound that increases according to an M^6 power law. Some additional measurements were also taken with two microphones, one located above the cylinder (as shown in Fig. 1 (a)) and one located directly below at same radial distance from the cylinder. The two microphone signals were found to be equal in magnitude and out-of-phase confirming the dipolar nature of the sound field.

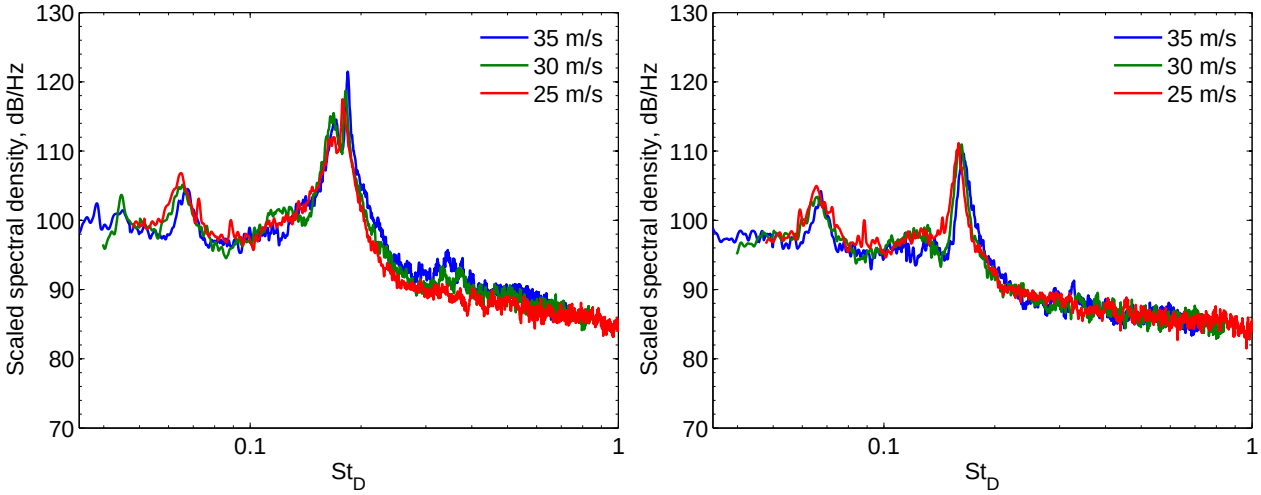

(a) Circular cylinder with $L/D = 22.6$.

(b) Circular cylinder with $L/D = 12.9$.

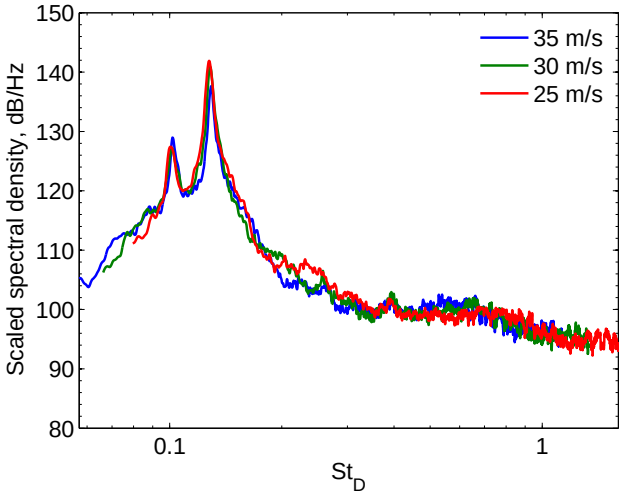

(c) Square cylinder with $L/D = 13.6$.

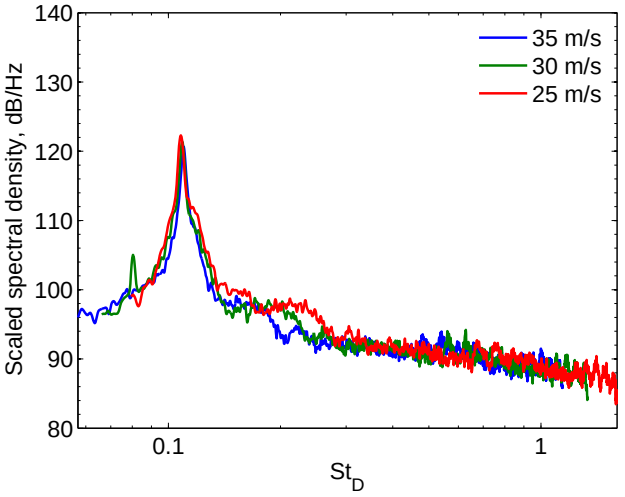

(d) Square cylinder with $L/D = 4.9$.

Figure 9: Scaled far-field acoustic spectra as a function of Strouhal number for the circular and square cylinder at $U_\infty = 25 - 35$ m/s.

4. Peak frequency scaling

Figure 10 shows the Strouhal number, St_D, of the dominant peaks in the cylinder noise spectra as a function of aspect ratio at flow speeds between $U_\infty = 25$ and 35 m/s. Also shown for comparison are the circular cylinder data of King and Pfizenmaier[21] for cylinders with a similar aspect ratio to those in this study.

Figure 10 shows cylinder aspect ratio has a significant effect on the Strouhal number of vortex shedding noise contributions. For the circular cylinders in this study, Fig. 10 (a) shows the dominant peak Strouhal numbers occur between 0.131 and 0.184 and increase with increasing aspect ratio. In comparison, King and Pfizenmaier[21] found vortex shedding noise contributions to occur at a higher Strouhal number of between 0.136 and 0.196 and their data displays a similar increase in Strouhal number with increasing aspect ratio.

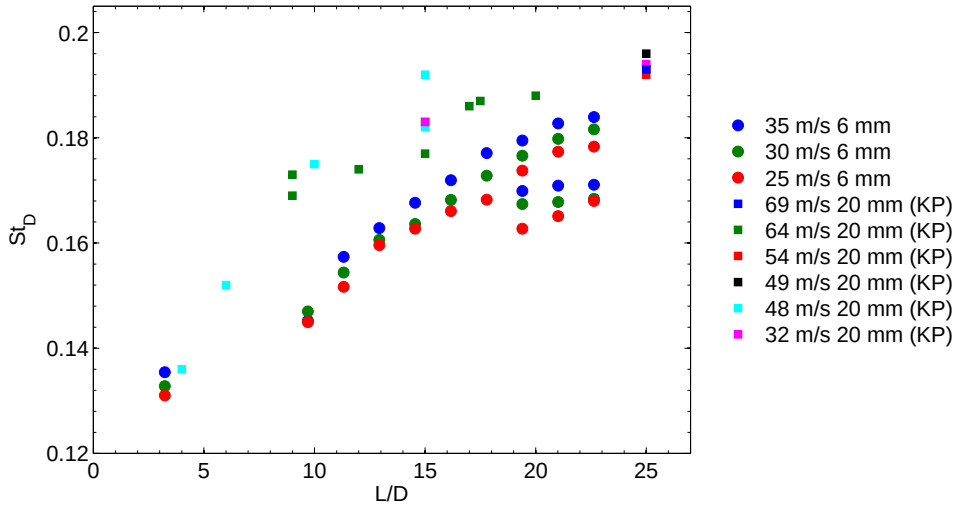

(a) Circular cylinder.

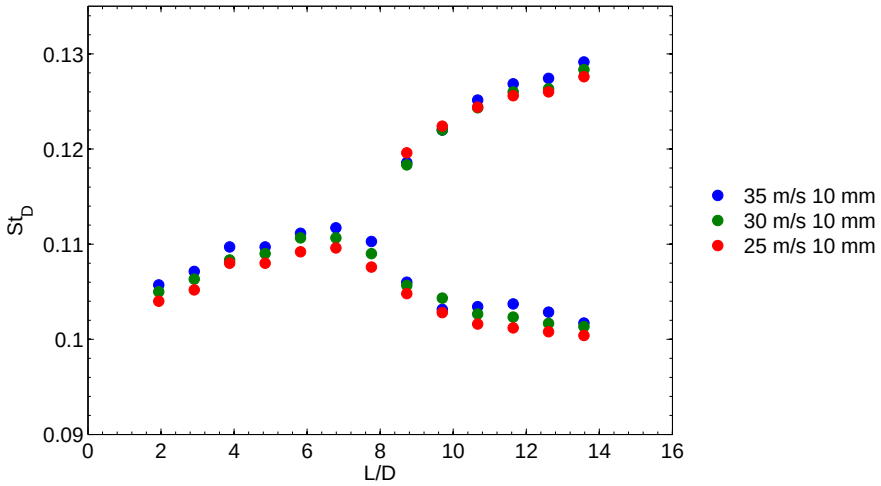

(b) Square cylinder.

Figure 10: Strouhal number versus aspect ratio for the circular and square cylinders at $U_\infty = 25 - 35$ m/s compared with the data of King and Pfizenmaier[21] (indicated by KP in legend). Legend indicates flow speed and cylinder diameter.

Differences in peak Strouhal number can be attributed to the fact that the study of King and Pfizenmaier[21] examined the noise radiated by finite height circular cylinders in a free jet and not in a turbulent boundary layer.

For the square cylinder in Fig. 10 (b), vortex shedding noise contributions occur at a Strouhal number of between 0.1 and 0.129. A clear junction exists at $L/D = 7.8$, above and below which dominant double and single peaks are observed in the noise spectra, respectively. For $L/D > 7.8$, the difference between the two Strouhal numbers of the double peak increases with aspect ratio while for $L/D < 7.8$, the Strouhal number associated with the single peak decreases with decreasing aspect ratio.

In the study of Becker et al.,[22] a wall-mounted square cylinder with an aspect ratio of $L/D = 6$ was found to produce a single acoustic tone with a Strouhal number of 0.104. This is in good agreement with the experimental results of Fig. 10 (b), despite the fact that Becker et al.[22] conducted their experiments at higher Reynolds numbers (yet still in the subcritical range) than in this study.

In the subcritical range, a two-dimensional circular cylinder is expected to produce an Aeolian tone with a Strouhal number of $St_D = 0.2$.[26] Figure 10 (a) shows that for the finite height circular cylinder in this study, vortex shedding noise contributions occur at a maximum Strouhal number of $St_D = 0.184$ at the highest

cylinder aspect ratio of $L/D = 22.6$. Vortex shedding therefore occurs at a lower Strouhal number for the finite height cylinder than for a two-dimensional cylinder in the subcritical range. This has been similarly observed in studies examining the turbulent flow field around finite height cylinders and is attributed to the influence of downwash flow and tip vortices at the cylinder free-end on spanwise vortex shedding from the cylinder sides.[11,16,27,28] According to Zdravkovich,[29] downwash at the free-end increases the vortex formation length and expands the near wake region, prolonging spanwise vortex shedding and reducing its associated frequency.

B. Wake velocity measurements

As the turbulent flow field around the cylinder is the source of sound radiated into the far-field, velocity measurements in the cylinder wake, taken simultaneously with acoustic measurements, are presented in this section to give insight into the mechanisms responsible for noise generation. While velocity measurements are presented at the selected flow speed of $U_\infty = 35$ m/s only, measurements at flow speeds to $U_\infty = 25$ m/s show identical information.

Figures 11 - 16 show 2D spectral maps of the power spectral density of the fluctuating velocity (u'^2/Hz) measured along the cylinder span for cylinders with selected aspect ratios. Also shown in these figures are 2D spectral maps of the coherence between the acoustic and velocity measurements. The velocity measurements have been taken at two and three diameters downstream of the circular and square cylinders in the x direction, respectively. This position was chosen so that the probe was placed well outside of the recirculation zone in the wake of the cylinder. A position of $y/L = 0$ corresponds to the cylinder wall-junction, while $y/L = 1$ corresponds to the cylinder free-end.

Figures 11 and 12 show wake velocity measurements for the circular cylinder with $L/D = 22.6$ and the square cylinder with $L/D = 13.6$. These cylinders both produce a dominant double peak in their corresponding far-field noise spectra (see Fig. 5 (a) and 6 (a)). The wake velocity measurements for both cylinders show the cylinder span is divided into two distinct regions of Karman vortex shedding with a different shedding frequency (and second harmonic) associated with each part. This cellular or piecewise variation in Karman vortex shedding along the cylinder span is responsible for the dominant double peak observed in the cylinder noise spectra.

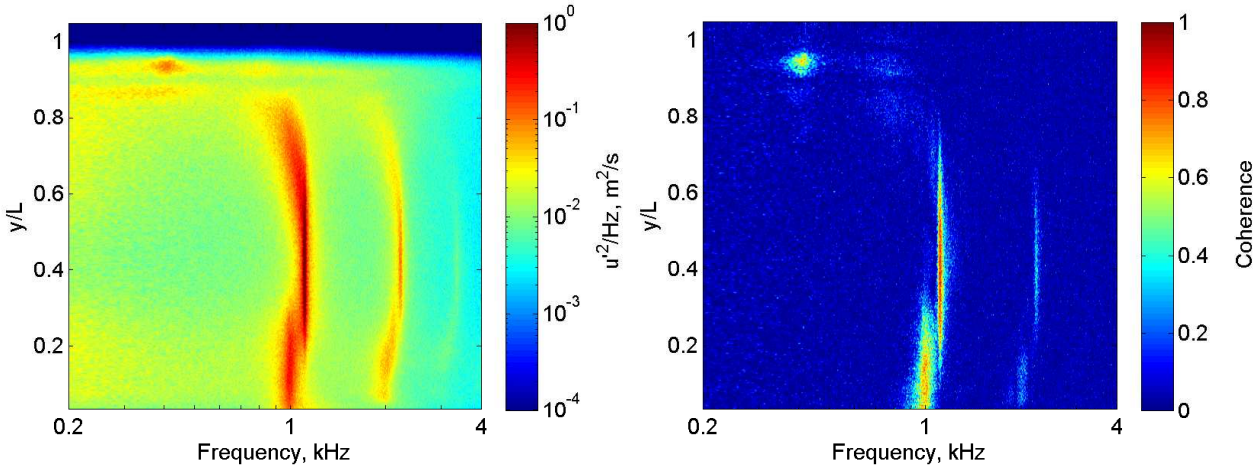

(a) Fluctuating velocity.

(b) Coherence.

Figure 11: Spectral maps of the power spectral density of the fluctuating velocity and coherence between the acoustic and velocity measurements for the circular cylinder with L/D = 22.6 at $U_\infty = 35$ m/s.

The noise spectrum of the circular cylinder with $L/D = 22.6$ in Figure 5 (a) displays a dominant double peak with peak frequencies of $f_1 = 998$ Hz and $f_2 = 1076$ Hz at $U_\infty = 35$ m/s. The velocity and coherence spectral maps for this cylinder in Figure 11 show vortex shedding occurs in the lower region of the cylinder span, near the cylinder-wall junction, at the lower dominant acoustic peak frequency of f_1. The cylinder mid region meanwhile, is characterised by vortex shedding at the higher dominant acoustic peak frequency of f_2. It is likely that vortex structures that form at the cylinder-wall junction and the associated upward-directed

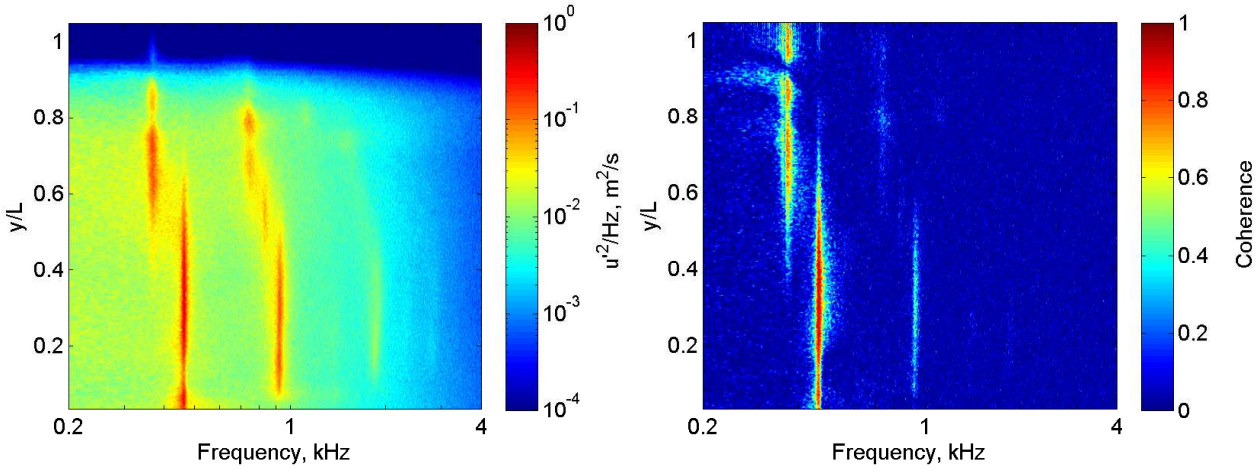

(a) Fluctuating velocity.

(b) Coherence.

Figure 12: Spectral maps of the power spectral density of the fluctuating velocity and coherence between the acoustic and velocity measurements for the square cylinder with L/D = 13.6 at $U_\infty = 35$ m/s.

flow interact with Karman vortex shedding in the cylinder's lower region, reducing the shedding frequency. As the aspect ratio of the cylinder is high, the cylinder is long enough to have a region of vortex shedding at mid span that occurs undisturbed by flow at the wall, resulting in a variation in shedding frequency along its span.

The noise spectrum of the square cylinder with $L/D = 13.6$ in Figure 6 (a) shows a dominant double peak with peak frequencies of $f_1 = 356$ Hz and $f_2 = 452$ Hz at $U_\infty = 35$ m/s. The velocity and coherence measurements in Figure 12 show this cylinder has an upper region, near its free-end, characterised by vortex shedding at the lower dominant acoustic peak frequency of f_1 and a mid-to-low region characterised by vortex shedding at the higher dominant acoustic peak frequency of f_2. In this case, downwash from the cylinder free-end interacts with vortex shedding from the sides of the cylinder near its tip, reducing the shedding frequency. As the cylinder has a large aspect ratio, vortex shedding at mid-to-low span occurs undisturbed by flow over the tip, resulting in a variation in shedding frequency along the cylinder span. In contrast to the circular cylinder, the junction flow at wall does not affect the vortex shedding frequency. Figure 11 shows downwash also has an effect on vortex shedding near the circular cylinder free-end but in this case it appears to weaken and suppress this vortex shedding process gradually rather than create the cellular vortex shedding behaviour observed for the square cylinder.

Figures 13 and 14 show wake velocity measurements for the circular cylinder with $L/D = 12.9$ and the square cylinder with $L/D = 4.85$. These cylinders both produce a dominant single peak in their corresponding far-field noise spectra (see Fig. 5 (b) and 6 (b)). The wake velocity measurements for both cylinders show vortex shedding occurs along the cylinder span at a single frequency (and its second harmonic) corresponding to that of the dominant single peak in the cylinder noise spectra. In this case, it is likely that the cylinder aspect ratio is low enough that upwash at the circular cylinder-wall junction and downwash at the square cylinder free-end have an influence along the entire cylinder span so that spanwise vortex shedding occurs at a single frequency, resulting in production of a single acoustic tone. The experimental results therefore suggest that the cellular structure of Karman vortex shedding reduces with cylinder aspect ratio moving from two cells (when $L/D > 19.4$ for the circular cylinder and $L/D > 8.7$ for the square cylinder) to one cell (when L/D is between 9.7 and 17.8 for the circular cylinder and between 7.8 and 1.9 for the square cylinder), resulting in a dominant double and single peak in the noise spectra, respectively.

The noise spectra for circular cylinders with aspect ratio between $L/D = 9.7$ and 22.6 show the dominant double and single peaks are accompanied by a low amplitude, low frequency secondary peak (see Figs. 5 (a) and (b)). The velocity measurements in Figs. 11 and 13 for circular cylinders with $L/D = 22.6$ and 12.9 show high intensity velocity fluctuations and high coherence between the acoustic and velocity signals at the secondary peak frequency near the cylinder tip. Hence, the secondary peak in the circular cylinder noise spectra is due to the formation of vortex structures at the cylinder tip. The velocity spectral maps in

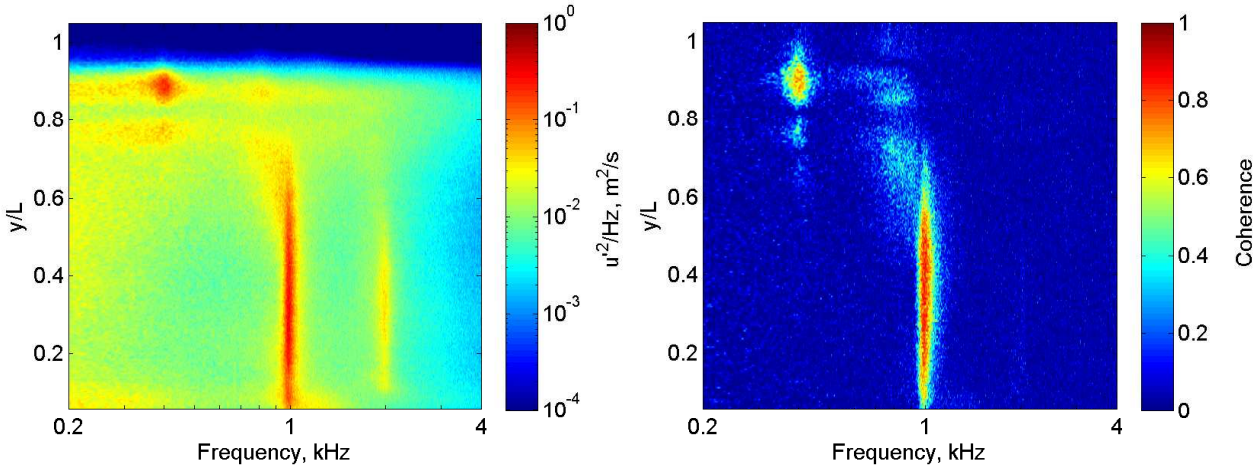

(a) Fluctuating velocity. (b) Coherence.

Figure 13: Spectral maps of the power spectral density of the fluctuating velocity and coherence between the acoustic and velocity measurements for the circular cylinder with L/D = 12.9 at $U_\infty = 35$ m/s.

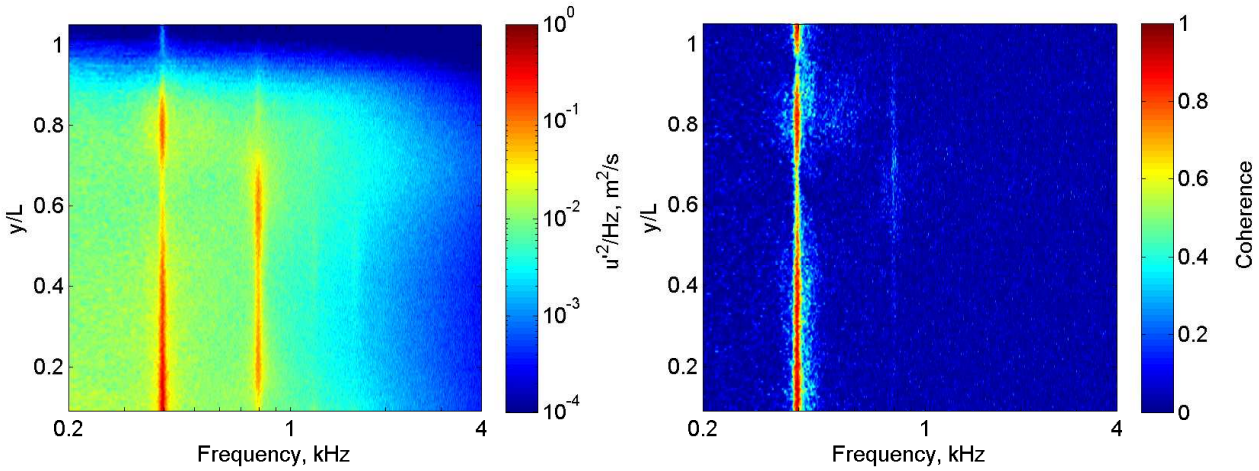

(a) Fluctuating velocity. (b) Coherence.

Figure 14: Spectral maps of the power spectral density of the fluctuating velocity and coherence between the acoustic and velocity measurements for the square cylinder with L/D = 4.85 at $U_\infty = 35$ m/s.

Figs. 12 (a) and 14 (a) for square cylinders with $L/D = 13.6$ and 4.85 were examined at frequencies down to 10 Hz and showed no evidence of vortex shedding at the cylinder tip. Correspondingly, no secondary peak is observed in the square cylinder noise spectra (see Figs. 6 (a) and (b)).

No peaks are observed in the noise spectra for circular cylinders with an aspect ratio between $L/D = 4.9$ and 8.1 (see Fig. 5 (c)) and for the square cylinder when $L/D = 0.97$ (see Fig. 6 (c)). In this case, vortex shedding is suppressed, preventing acoustic tone generation. This is confirmed by examining the wake velocity measurements for the circular cylinder with aspect ratio of $L/D = 6.5$ in Fig. 15. This figure shows the flow field along the cylinder span is composed of broadband random velocity fluctuations and correspondingly, the cylinder does not radiate any tonal noise components (see Fig. 5 (c)).

A single peak reappears in the noise spectra for the circular cylinder with aspect ratio of $L/D = 3.2$ (see Fig. 5 (d)). The velocity measurements for this cylinder in Fig. 16 show high intensity velocity fluctuations and high coherence between the acoustic and velocity signals at the peak frequency occur near the cylinder-wall junction. This indicates that vortex shedding from the cylinder's lower region is responsible for the

single acoustic tone produced by this cylinder.

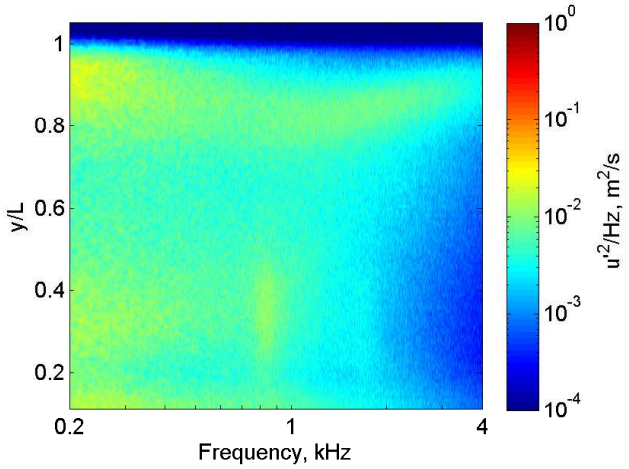

Figure 15: Spectral map of the power spectral density of the fluctuating velocity for the circular cylinder with L/D = 6.5 at $U_\infty = 35$ m/s.

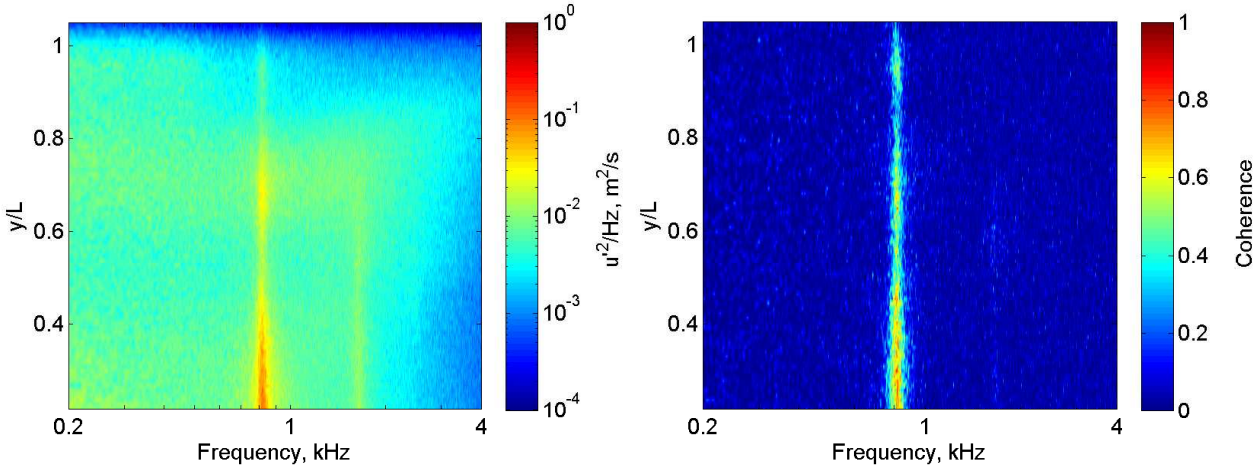

(a) Fluctuating velocity.

(b) Coherence.

Figure 16: Spectral maps of the power spectral density of the fluctuating velocity and coherence between the acoustic and velocity measurements for the circular cylinder with L/D = 3.2 at $U_\infty = 35$ m/s.

IV. Conclusion

This paper has presented results of an experimental investigation of the noise produced by flow interaction with a wall-mounted finite length cylinder of circular and square cross-section. The results include far-field acoustic measurements and velocity spectra measured in the cylinder wake at a number of flow speeds and for a variety of cylinder aspect ratios.

Flow speed was shown to influence the overall sound pressure level and peak Strouhal number. The dipole scaling law of M^6 gave a good collapse of the far-field noise spectra produced by cylinders with both circular and square cross-section, demonstrating that the radiated sound field has dipole like radiation characteristics.

Aspect ratio was found to be an important parameter that determines how or whether vortices are shed from the cylinder resulting in acoustic tone generation. Multiple tones are attributed to a cellular variation in vortex shedding along the cylinder span. The number of vortex cells is dependent on aspect ratio as this

parameter determines the proportion of the cylinder span influenced by flow over the cylinder-wall junction or tip. For cylinders with high aspect ratio ($L/D > 19.4$ for the circular cylinder and $L/D > 8.7$ for the square cylinder), two vortex cells are observed and correspondingly, two dominant acoustic tones are produced. In this case, vortex shedding at mid span appears to be undisturbed by flow at the cylinder-wall junction or tip, resulting in a variation in shedding frequency along the cylinder span. At lower aspect ratio (when L/D is between 9.7 and 17.8 for the circular cylinder and between 7.8 and 1.9 for the square cylinder), only a single vortex cell and one dominant acoustic tone are observed. In this case, end-effects are expected to influence the entire cylinder span so that spanwise vortex shedding occurs at a single frequency. No vortex shedding was observed for cylinders with very low aspect ratio (for circular cylinders with $L/D = 4.9$ between 8.1 and for square cylinders with $L/D = 0.97$) and the sound radiated into the far-field is low and broadband in nature.

Acknowledgments

This work has been supported by the Australian Research Council under linkage grant LP110100033 'Understanding and predicting submarine hydrofoil noise'.

References

[1]Curle, N., "The influence of solid boundaries upon aerodynamic sound," *Proceedings of the Royal Society of London A: Mathematical, Physical and Engineering Sciences*, Vol. 231, 1955, pp. 505–514.

[2]Gerrard, J., "Measurements of the sound from circular cylinders in an air stream," *Proceedings of the Royal Society of London, Series B*, Vol. 68, 1955, pp. 453–461.

[3]Phillips, O., "The intensity of Aeolian tones," *Journal of Fluid Mechanics*, Vol. 607 - 624, 1, pp. 1956.

[4]Schlinker, R., Fink, M., and Amiet, R., "Vortex noise from non-rotating cylinders and airfoils," *AIAA 14th Aerospace Sciences Meeting*, Washington, D.C., January 26 28 1976.

[5]Cox, J., Brentner, K., and Rumsey, C., "Computation of vortex shedding and radiated sound for a circular cylinder: subcritical to transcritical Reynolds numbers," *Theoretical and Computational Fluid Dynamics*, Vol. 12, 1998, pp. 233 – 253.

[6]Inoue, O. and Hatakeyam, H., "Sound generation by a two-dimensional circular cylinder in a uniform flow," *Journal of Fluid Mechanics*, Vol. 471, 2002, pp. 285 – 314.

[7]Fujita, H., Suzuki, Y., Itou, T., and Hashimoto, Y., "The characteristics of the flow field around two-dimensional cylinders in relation to the Aeolian tone generation," *Internoise 2006*, Honolulu, Hawaii, December 3 - 6 2006.

[8]Cheong, C., Joseph, P., Park, Y., and Lee, S., "Computation of Aeolian tone from a circular cylinder using source models," *Applied Acoustics*, Vol. 69(2), 2008, pp. 110 – 126.

[9]Ali, M., Doolan, C., and Wheatley, V., "Low Reynolds number flow over a square cylinder with a splitter plate," *Physics of Fluids*, Vol. 23(3), 2011.

[10]Ali, M., Doolan, C., and Wheatley, V., "Aeolian tones generated by a square cylinder with a detached flat plate," *17th AIAA/CEAS Aeroacoustics Conference*, Portland Oregon, June 5 - 8 2011.

[11]Kawamura, T., Hiwada, M., Habino, T., Mabuchi, L., and Kumada, M., "Flow around a finite circular cylinder on a flat plate," *Bulletin of the Japan Society of Mechanical Engineers*, Vol. 27, 1984, pp. 2142–2150.

[12]Lee, L., "Wake structure behind a circular cylinder with a free end," *Proceedings of the Heat Transfer and Fluids Mechanics Institute*, 1997, pp. 241–251.

[13]Park, W. and Lee, S., "Effects of free-end corner shaped on flow structure around a finite cylinder," *Journal of Fluids and Structures*, Vol. 19, 2004, pp. 141–158.

[14]Kirkil, G. and Constantinescu, G., "A numerical study of the laminar necklace vortex system and its effect on the wake for a circular cylinder," *Physics of Fluids*, Vol. 24, 2012.

[15]Tanaka, S. and Murata, S., "An inverstigation of the wake structure and aerodynamic characteristics of a finite circular cylinder," *JSME International Journal*, Vol. 42(2), 1999, pp. 178–187.

[16]Sumner, D., Heseltine, J., and Dansereau, O., "Wake structure of a finite circular cylinder of small aspect ratio," *Experiments in Fluids*, Vol. 37, 2004, pp. 720–730.

[17]Wang, H. and Zhou, Y., "The finite-length square cylinder near wake," *Journal of Fluid Mechanics*, Vol. 638, 2009, pp. 453–490.

[18]Rostamy, N., Sumner, D., Bergstrom, D., and Bugg, J., "Local flow field of a surface-mounted finite circular cylinder," *Journal of Fluids and Structures*, Vol. In Press, 2012, In Press.

[19]Sakamoto, H. and Arie, M., "Vortex shedding from a rectangular prism and a circular cylinder placed vertically in a turbulent boundary layer," *Journal of Fluid Mechanics*, Vol. 126, 1983, pp. 147–165.

[20]Okamoto, S. and Sunabashiri, Y., "Vortex shedding from a circular cylinder of finite length placed on a ground plane," *Transactions ASME, Journal of Fluid Engineering*, Vol. 114, 1992, pp. 512–521.

[21]King, W. and Pfizenmaier, E., "An experimental study of sound generated by flows around cylinders of different cross-section," *Journal of Sound and Vibration*, Vol. 328, 2009, pp. 318–337.

[22]Becker, S., Hahn, C., Kaltenbacher, M., and Lerch, R., "Flow-induced sound of wall-mounted cylinders with different geometries," *AIAA Journal*, Vol. 46(9), 2008, pp. 2265 – 2281.

[23]Moreau, D., Brooks, L., and Doolan, C., "Broadband trailing edge noise from a sharp-edged strut," *Journal of the Acoustical Society of America*, Vol. 129(5), 2011, pp. 2820 –2829.

[24]Roshko, A., "Experiments on the flow past a circular cylinder at very high Reynolds number," *Journal of Fluid Mechanics*, Vol. 10 (2), 1961, pp. 345 – 356.

[25]Cebeci, T. and Bradshaw, P., *Momentum Transfer in Boundary Layers*, Hemisphere Publishing Corporation, Washington, 1977.

[26]Norberg, C., "Fluctuating lift on a circular cylinder: review and new measurements," *Journal of Fluids and Structures*, Vol. 17, 2003, pp. 57 – 96.

[27]Farivar, D., "Turbulent uniform flow around cylinders of finite length," *AIAA Journal*, Vol. 19, 1981, pp. 275–281.

[28]Park, C. and Lee, S., "Free end effects on the near wake flow structure behind a finite circular cylinder," *Journal of Wind Engineering and Industrial Aerodynamics*, Vol. 88, 2000, pp. 231–246.

[29]Zdravkovich, M., *Flow around circular cylinders, volume 2: applications*, Oxford University Press, 2003.